



1 **The value of water isotope data on improving process**  
2 **understanding in a glacierized catchment on the Tibetan**  
3 **Plateau**

4 Yi Nan<sup>1</sup>, Lide Tian<sup>2,3</sup>, Zhihua He<sup>4</sup>, Fuqiang Tian<sup>1</sup>, Lili Shao<sup>2</sup>

5 <sup>1</sup>Department of Hydraulic Engineering, State Key Laboratory of Hydrosience and Engineering,  
6 Tsinghua University, Beijing 100084, China

7 <sup>2</sup>Institute of International Rivers and Eco-security, Yunnan University, Kunming, China

8 <sup>3</sup>CAS Center of Excellence in Tibetan Plateau Earth Sciences, Beijing 100101, China

9 <sup>4</sup>Center for Hydrology, University of Saskatchewan, Saskatchewan, Canada

10 **Corresponding to:** Fuqiang Tian

11 Address: Room 330 New Hydraulic Building, Tsinghua University, Beijing 100084, China

12 Email: [tianfq@mail.tsinghua.edu.cn](mailto:tianfq@mail.tsinghua.edu.cn)

13

14

15

16



17 **Abstract**

18 This study integrated a water isotope module into the hydrological model THREW which has been  
19 successfully used in high and cold regions. Signatures of oxygen stable isotope ( $^{18}\text{O}$ ) of different water  
20 inputs and stores were simulated coupling with the simulations of runoff generations. Isotope  
21 measurements of precipitation water samples and global precipitation isotope product, as well as assumed  
22 constant isotope signature of ice meltwater were used to force the isotope module. Isotope signatures of  
23 water stores such as snowpack and subsurface water were updated by an assumed completely mixing  
24 procedure. Fractionation effects of snowmelt and evapotranspiration were modeled in a Rayleigh  
25 fractionation approach. The isotope-aided model was subsequently applied for the quantifications of  
26 runoff components and estimations of mean water travel time (MTT) and mean residence time (MRT) in  
27 the glacierized watershed of Karuxung River on the Tibetan Plateau. Model parameters were constrained  
28 by three different combinations of observations including a single-objective calibration using streamflow  
29 measurement solely, a dual-objective calibration using both streamflow measurement and MODIS  
30 estimated snow cover area, and a triple-objective calibration using additionally isotopic composition of  
31 stream water. Modeled MTT and MRT was validated by estimate of a tracer-based sine-wave method.  
32 Results indicate that: (1) the proposed model performed quite well on simultaneously reproducing the  
33 observations of streamflow, snow cover area, and isotopic composition of stream water, despite that only  
34 precipitation water samples were available for tracer input; (2) isotope data helped to estimate more  
35 plausible contributions of runoff components (CRCs) to streamflow in the melting season, and improved  
36 the robustness of MTT and MRT estimations; (3) involving isotope data for the model calibration  
37 obviously reduced uncertainties of the quantification of CRCs and estimations of MTT and MRT, through  
38 better constraining the strong competitions among different runoff processes induced by meltwater and  
39 rainfall. Our results inform high value of water isotope data on improving process understanding in a  
40 glacierized basin on the Tibetan Plateau.

41 **Keywords:**

42 Tracer-aided hydrological model; Contribution of runoff components; Water travel time; Glacierized  
43 catchment; Tibetan Plateau

44

45



## 46 1. Introduction

47 The Tibetan Plateau as a high mountainous cryosphere is the source of many major rivers in Asia  
48 including Yarlung Tsangpo-Brahmaputra River, Ganges River, Indus River and so on (Report of STEP,  
49 2018). Scientific understanding of hydrological processes in this region is critical in predicting the  
50 responses of water resources and water hazards to climate changes (Lutz et al., 2014; Immerzeel et al.,  
51 2010; Miller et al., 2012). River runoff in these basins is prominently fed by multiple water sources  
52 including snowmelt, glacier melt and rainfall (Li et al., 2019). Coupling with the strong spatio-temporal  
53 variabilities of meteorological inputs, the complicated runoff generation processes imply big challenges  
54 in understanding the hydrological behaviors in glacierized basins on the Tibetan Plateau.

55 It is, therefore, of critical importance to quantify contributions of runoff components (CRCs) to  
56 streamflow in glacierized regions. Estimating CRCs by hydrological models is one of the commonly  
57 adopted method (Weiler et al. 2018), which is particularly subject to the following challenges. First,  
58 modeled CRCs rely heavily on the model conceptualizations of the mixing and propagations of different  
59 water sources in the basin. Model configurations and corresponding parameters representing the storage  
60 capacities of soil layers and groundwater aquifers obviously affect the relative proportions of surface and  
61 subsurface flow to streamflow (Nepal et al. 2014). CRCs modeled by different hydrological models are  
62 thus rarely comparable (Tian et al. 2020). For example, Nepal et al. (2015) and Siderius et al. (2013)  
63 compared CRCs estimated by different glacio-hydrological models in glacierized basins in the  
64 Himalayan region, and demonstrated considerable variations of the modeled CRCs. They attributed the  
65 difference to the variations of the model conceptualizations. Second, strong compensatory effects of the  
66 simulated runoff induced by precipitation and ice meltwater which were typically not well constrained  
67 in the model resulted in large variations of the modeled CRCs. For instance, modeling results from  
68 Duethmann et al. (2015) and Finger et al. (2015) indicated that overestimated precipitation-triggered  
69 runoff in the model can be easily compensated by an underestimated ice melt runoff and vice versa,  
70 especially in high altitude glacierized basins where precipitation input have large uncertainty.

71 Tracer data of water stable isotope have been widely used to label runoff components in the popular  
72 end-member mixing approach (e. g., Kong et al. 2011; He et al. 2020). Its value for improving modeled  
73 CRCs, however, have not been sufficiently investigated. Previous applications of tracer-aided  
74 hydrological models which integrated the simulation of water isotopic compositions of different runoff  
75 components into the rainfall/melting-runoff processes in snow dominated basins have demonstrated high  
76 values of water isotope data on diagnostically improving model structure and recognizing the dominances  
77 of runoff processes on streamflow (Capell et al., 2012; Delavau et al. 2017; Son and Sivapalan, 2007;  
78 Birkel et al., 2011; Stadnyk and Holmes, 2020). An early test of the isotope-aided hydrological model in  
79 a glacierized basin in Tianshan Central Asia of He et al. (2019) indicated that additionally use of isotope  
80 data helped to constrain the internal apportionments of runoff components in the model and improved  
81 the estimation of CRCs at an event scale. However, exploring the values of water isotope data for  
82 hydrological modelling in glacierized basins are still limited to the low availability of water tracer data  
83 from field water sampling due to the harsh environment, especially for glacierized basins on the Tibetan  
84 Plateau. As far as we know, glacio-hydrological model coupled with the simulations of isotope signatures  
85 have not been developed and tested in the Tibetan Plateau yet.

86 Quantifying the time from entrance of water to its exits is fundamental to understandings of flow  
87 pathways and the storage and mixing processes (McGurie and McDonnell, 2006). Characterizing water  
88 travel time distribution (TTD) and mean travel time (MTT) in addition to the traditional focus on



89 streamflow response allows us to be closer to getting the right answers for the right reasons (Hrachowitz  
90 et al. 2013). Despite that TTD and MTT serve good tools to diagnose unsuitable model structures and  
91 parameterizations (McMillan et al. 2012), it has been rarely quantified in glacierized basins. Plenty of  
92 convenient tools have been developed based on lumped parameter models, but their practical applications  
93 in glacierized basins are restricted by the time invariant assumption and the weakness on considering the  
94 strong spatio-temporal variability of runoff processes (van Huijgevoort et al. 2016) as well as the seasonal  
95 water inputs from snowmelt and glacier melt. Fully physically-based water particle tracking approaches  
96 coupling with hydrological processes whereas are only limited to small basins due to the heavy  
97 computation cost (Remondi et al. 2018). Conceptual models that used additional tracer storage  
98 compartments along with the flow and transport processes have provided crucial information on the  
99 dynamics of flow pathways and storages, but rely heavily on the prior definitions of function shape (e.g.,  
100 travel time distribution (TTD) in van der Velde et al. 2015; StorAge Selection function (SAS) in Benettin  
101 and Bertuzzo 2018; age-ranked storage-discharge relation in Harman 2019). In contrast, tracer-aided  
102 hydrological models that integrated the storage and transportation of conservative water tracers into the  
103 runoff generation processes have been demonstrated as successful on estimating TTD and water ages as  
104 well as their time variances with in snowmelt influenced basins (e.g., Soulsby et al. 2015; Ala-Aho  
105 et al. 2017). However, such hydrological models have not been applied in glacierized basins for estimations  
106 of TTD and MTT yet.

107 For process understanding in glacierized basins, glacio-hydrological models that additionally  
108 represented the snow processes and glacier evolution have been widely used (e.g. Immerzee et al. 2013;  
109 Lutz et al. 2014 and 2016; Luo et al. 2018). The more complex integration of water sources from different  
110 flow pathways and units whereas resulted in expanded parameter space of these hydrological models  
111 which introduced large uncertainty in the model calibration (Finger et al. 2015). Equifinality is serious  
112 in these regions when calibrating hydrological model by streamflow solely, indicating that different  
113 parameters and runoff component proportions could perform similarly in discharge simulation (Beven  
114 and Freer, 2001; Chen et al., 2017), despite of the general good performance for streamflow simulation.  
115 Therefore, multiple datasets including glacier observation and remotely sensed snow products have been  
116 frequently used in addition to streamflow measurements in vast glacio-hydrological simulations (e.g.,  
117 Parajka and Blöschl, 2008; Konz and Seibert, 2010; Schaeffli and Huss 2011; Duethmann et al. 2014;  
118 Finger et al., 2015; He et al. 2018). However, both discharge and snow/glacier measurements provide  
119 insufficient constraints on distributions of flow pathways and the parameterizations of subsurface water  
120 storages (He et al. 2019). Although application in a glacierized basin in Central Asia of He et al. (2019)  
121 indicated high utility of isotope data on constraining the complex interactions of multiple runoff  
122 processes for the quantifications of CRCs, the values of water tracer such as stable isotope on reducing  
123 uncertainties on the estimations of TTD and MTT in glacierized basins on Tibetan Plateau have not been  
124 investigated.

125 In light of those backgrounds, this study integrated the simulation of oxygen isotope signatures into  
126 a hydrological model that has been proved effective to simulate the runoff processes on the Tibetan  
127 Plateau. The developed tracer-aided hydrological model was applied to the Karuxung River catchment  
128 (286 km<sup>2</sup>, 4550 to 7206 m a.s.l.) on Tibetan Plateau. The objectives of this study are: (1) to test the  
129 capability of the proposed tracer-aided model on simultaneously reproducing streamflow and isotope  
130 signatures of stream water in the study basin where only precipitation water samples are available for  
131 isotope input, (2) to evaluate the values of tracer-aided method on improving the estimation of CRCs and  
132 TTD/MTT in the study basin, and (3) to assess and interpret the differences between modeled TTD/MTT



133 and estimates by a lumped parameter method.

## 134 **2. Materials and methodology**

### 135 **2.1 Study area and data**

136 This study focuses on the Karuxung catchment, which is located in the upper region of the Yarlung  
137 Tsangpo River basin, on the northern slope of the Himalayan Mountains (Figure 1). Digital elevation  
138 model (DEM) data in the study catchment with a spatial resolution of 30-m was downloaded from the  
139 Geospatial Data Cloud ([www.gscloud.cn](http://www.gscloud.cn)). The Karuxung river originates from the Lejin Jangsan Peak  
140 of the Karola Mountain at 7206 m above sea level (a.s.l.), and flows into the Yamdrok Lake at 4550m  
141 a.s.l. (Zhang et al., 2006). The catchment covers an area of 286 km<sup>2</sup>. The river discharge is significantly  
142 influenced by the headwater glaciers which cover an area of around 58 km<sup>2</sup> (Mi et al., 2001). This  
143 catchment is dominated by a semi-arid climate. The mean annual temperature and precipitation at  
144 Langkazi Weather Station were 3.4°C and 379 mm, respectively. Due to the effect of the South Asian  
145 Monsoon, more than 90% of the annual precipitation falls between June and September. Precipitation  
146 occurs mostly in form of snow from October to the following March at high elevations (Zhang et al.,  
147 2015).

148 **[Figure 1]**

149 Daily temperature and precipitation data from 1<sup>st</sup> January 2006 to 30<sup>th</sup> September 2012 were  
150 collected at the Langkazi Weather Station (4432 m a.s.l.). Altitudinal distributions of temperature and  
151 precipitation across the catchment were estimated by the lapse rates reported in Zhang et al. (2015).  
152 Runoff were measured daily from 1<sup>st</sup> April 2006 to 31<sup>st</sup> December 2012 at the Wengguo Hydrological  
153 Station at the catchment outlet. The coverages of glaciers were extracted from the Second Glacier  
154 Inventory Dataset of China (Liu, 2012). The 8-day snow cover extent data from MODIS product of  
155 MOD10A2 (500m×500m, Hall and Riggs, 2016) were used to denote the fluctuations of the snow cover  
156 area (SCA). The 8-day Leaf Area Index (LAI) and the monthly normalized difference vegetation index  
157 (NDVI) data were downloaded from MODIS product of MOD15A2H (500m×500m, Myneni et al., 2015)  
158 and MOD13A3 (1km×1km, Didan, 2015). Soil hydraulic parameters were estimated based on the soil  
159 properties extracted from the 1km × 1km Harmonized World Soil Database (HWSD,  
160 <http://www.fao.org/geonetwork/>).

161 Grab samples of precipitation and stream water were collected at the Wengguo Station in 2006-  
162 2007 and 2010-2012, for analysis of  $\delta^{18}\text{O}$  and  $\delta^2\text{H}$ , and the characteristics of samples are summarized in  
163 Table1. In the dry seasons when precipitation water was not sampled due to small event amounts,  
164 precipitation isotope data from monthly Regionalized Cluster-based Water Isotope Prediction (RCWIP  
165 with a pixel size of 10'×10', Terzer et al., 2013) were used as proxy for model input. The effect of  
166 elevation on the isotopic composition of precipitation was estimated using a lapse rate of -0.34‰/100m  
167 based on Liu et al. (2007). The stream water samples were collected weekly every Monday from the river  
168 channel near the Wengguo Station. Isotopic composition of glacier meltwater was assumed to be constant  
169 during the entire study period and the value reported in Gao et al. (2009) was adopted.

170 **[Table 1]**

### 171 **2.2 Tracer-aided hydrological model**

172 The THREW (Tsinghua Representative Elementary Watershed) model was originally developed by



173 Tian et al. (2006), and has been successfully applied to a wide range of catchments (e.g., Tian et al., 2012;  
174 Yang et al., 2014), including glacierized basins in the Alps, Tianshan, and the Tibet Plateau (He et al.,  
175 2014; 2015; Xu et al., 2019). The THREW model uses the Representative Elementary Watershed (REW)  
176 method for the spatial discretization of catchment, in which the study catchment is divided into REWs  
177 based on the catchment DEM, and then each of the REWs is divided into sub-zones as the basic units for  
178 hydrological simulation. More details of the model set up are given in Tian et al. (2006). In this study,  
179 the Karuxung catchment was divided into 41 REWs.

180 Meltwater from snow and glacier are simulated using a temperature-index method as given in Eqs.  
181 (1) and (2):

$$182 \quad M_N = \begin{cases} DDF_N * (T - T_{N0}) & \text{for } T > T_{N0} \\ 0 & \text{for } T \leq T_{N0} \end{cases} \quad (1)$$

$$183 \quad M_G = \begin{cases} DDF_G * (T - T_{G0}) & \text{for } T > T_{G0} \\ 0 & \text{for } T \leq T_{G0} \end{cases} \quad (2)$$

184 where, the subscripts  $N$  and  $G$  represent snow and glacier, respectively.  $M$  is the melt amount,  $T$  is  
185 temperature and  $T_0$  refers to temperature threshold above which snow/ice starts to melt.  $DDF$  is the  
186 degree-day factor, representing the melt rate. Glacier meltwater ( $M_G$ ) in this study includes both ice melt  
187 and snowmelt on the glacierized area.

188 The fraction of snowfall ( $P_N$ ) of the total precipitation  $P$  is determined by a temperature threshold  
189  $T_N$  in Eq. 3. Snow water equivalent (SWE) of each REW is thus updated by Eq. 4. The snow cover area  
190 (SCA) of the corresponding REW is determined by a SWE threshold value ( $SWE_0$ ): when the calculated  
191 SWE is higher than  $SWE_0$ , the SCA of this REW is recorded as 1, otherwise the SCA is assumed to be 0  
192 (similarly to Parajka and Blöschl, 2008; Zhang et al., 2015; He et al., 2014). The SCA of the whole study  
193 catchment is calculated as the ratio of the sum of the areas of snow covered REWs to the total catchment  
194 area. Values of  $T_N$  and  $SWE_0$  are set based on prior knowledge from Dou et al. (2011), Marques et al.  
195 (2011) and He et al. (2014):  $T_N = 2^\circ\text{C}$ ,  $SWE_0 = 20\text{mm}$ .

$$196 \quad P_N = \begin{cases} 0 & T \leq T_N \\ P & T > T_N \end{cases} \quad (3)$$

$$197 \quad \frac{dSWE}{dt} = P_N - M_N \quad (4)$$

198 Meltwater of ice and snow, and rainfall over the glacier area are assumed to flow directly into the  
199 channel near the glacier tongue in form of surface runoff, based on the low permeability of the glacier  
200 surface. Snowmelt in the non-glacier area is assumed to generate runoff in a similar way to rainfall  
201 (Schaefer et al., 2005). For model simplicity, the evolution of the glacier area is not simulated in the model  
202 for the short simulation period of five years.

203 Simulation of  $\delta^{18}\text{O}$  of multiple water sources was integrated into the runoff generation processes  
204 in the THREW model (hereafter abbreviated as a THREW-t model). The  $\delta^{18}\text{O}$  of water sources in each  
205 of the sub-zones was assumed to be conservative, meaning that no chemical reactions occurred during  
206 the mixing of water sources. We assumed that the isotopic compositions of precipitation and glacier  
207 meltwater are linearly dependent on elevation, and used linear gradients reported in Liu et al. (2007)  
208 to estimate the initial isotopic compositions of precipitation and glacier meltwater in individual REWs  
209 (similarly to He et al. 2019). The isotopic compositions of the snowpack and subsurface water storages



210 were initialized by a “spin-up” running for three hydrological years, assuming the isotopic  
 211 compositions of water storages would reach steady levels after three years’ running. Isotope  
 212 composition of event snowfall on the snowpack was assumed to be the same as that of precipitation  
 213 occurring in the corresponding REW.

214 The fractionation effects of evaporation on isotope composition of water were estimated by a  
 215 Rayleigh fractionation method in Eqs. (5) to (7) (Hindshaw et al., 2011; Wolfe et al., 2007; He et al.,  
 216 2019):

$$217 \quad \delta^{18}O_x' = \delta^{18}O_x * \frac{1-f^{CF(\frac{1}{\alpha}-1)+1}}{1-f} \quad (5)$$

$$218 \quad \ln\alpha = -0.00207 + \frac{-0.4156}{T} + \frac{1137}{T^2} \quad (6)$$

$$219 \quad f = 1 - \frac{w_x'}{w_x} \quad (7)$$

220 where,  $\delta^{18}O_x'$  is the isotope composition of the evaporated water,  $\delta^{18}O_x$  is the isotope composition of  
 221 water before evaporation,  $\alpha$  is the Rayleigh fractionation factor,  $T(K)$  is air temperature in the  
 222 corresponding catchment unit,  $CF$  is a correction factor, and  $f$  is the ratio of remaining water volume to  
 223 the original water volume before evaporation.

224 A complete mixing assumption was used for the tracer signatures in each water storage.  
 225 Consequently,  $\delta^{18}O$  of soil water and groundwater were updated according to the following equation:

$$226 \quad \delta^{18}O_t = \frac{w_o\delta^{18}O_o + \sum w^i\delta^{18}O^i}{w_o + \sum w^i} \quad (8)$$

227 where,  $w_o$  and  $\delta^{18}O_o$  are the water quantity and isotopic composition of the subsurface storages at the  
 228 prior step, respectively.  $w^i$  refers to the infiltration into the soil storage from water source  $i$ . For  
 229 groundwater storage,  $w^i$  refers to the seepage from upper soil water.  $\delta^{18}O^i$  stands for the isotopic  
 230 composition of input water source  $i$ .

231 Stream water in each of the REWs was considered as a mixture of three components including  
 232 inflow from the upstream REWs, runoff generated in the current REW, and the water storage in the  
 233 river channel. Consequently, the isotopic composition of stream water in each REW ( $\delta^{18}O_r$ ) was  
 234 estimated based on the following conservative mixing equation:

$$235 \quad \delta^{18}O_r = \frac{\delta^{18}O_{r0} * w_r + \sum \delta^{18}O_{r,up}^k * I^k + \delta^{18}O_{sur}R_{sur} + \delta^{18}O_{gw}R_{gw}}{w_r + \sum I^k + R_{sur} + R_{gw}} \quad (9)$$

236 where,  $\delta^{18}O_{r0}$  is the isotopic composition of stream water and  $w_r$  is the water storage in the river  
 237 channel at the time step before the mixing of runoff components.  $\delta^{18}O_{r,up}^k$  is the isotopic composition  
 238 of stream water coming from the upstream REW  $k$ , and  $I^k$  is the inflow from the corresponding  
 239 upstream REW. Subscripts of  $sur$  and  $gw$  refer to the surface runoff and subsurface flow from  
 240 groundwater outflow generated in the current REW.

### 241 2.3 Model calibration

242 The physical meaning and value ranges of the calibrated parameters in the THREW-t model are  
 243 described in Table 2. Parameter values were optimized using three calibration variants: (1) single-



244 objective calibration using only the observed discharge at the catchment outlet, (2) dual-objective  
245 calibration using both observed discharge and MODIS SCA estimates, and (3) triple-objective calibration  
246 using observed discharge, MODIS SCA estimates and  $\delta^{18}\text{O}$  measurements of stream water. Considering  
247 the data availability, we chose April 1<sup>st</sup> 2006 to December 31<sup>st</sup> 2010 as the calibration period, and January  
248 1<sup>st</sup> 2011 to September 30<sup>th</sup> 2012 as the validation period. For SCA, we used only the MODIS SCA  
249 estimates during the ablation period (1<sup>st</sup> May to 30<sup>th</sup> July) of each year for the model calibration, because  
250 simulations of runoff processes are mostly sensitive to the dynamics of snow cover extent in the melting  
251 period (Duethmann et al., 2014). Only the  $\delta^{18}\text{O}$  measurements of stream water in the rainy season (from  
252 the first rainfall event to the last rainfall event of each year, as shown in Table 1) were used to optimize  
253 the model parameters, because the measured isotope data for precipitation were only available in this  
254 season. We chose the objective functions of Nash Sutcliffe efficiency coefficient (NSE) (Nash and  
255 Sutcliffe, 1970) and mean absolute error (MAE) to optimize the simulations of discharge, SCA and  
256 isotope respectively (Eqs. 12-14).

$$257 \quad NSE_{dis} = 1 - \frac{\sum_{i=1}^n (Q_{o,i} - Q_{s,i})^2}{\sum_{i=1}^n (Q_{o,i} - \overline{Q_o})^2} \quad (10)$$

$$258 \quad MAE_{SCA} = \frac{\sum_{i=1}^n |SCA_{o,i} - SCA_{s,i}|}{n} \quad (11)$$

$$259 \quad MAE_{iso} = \frac{\sum_{i=1}^n |\delta^{18}O_{o,i} - \delta^{18}O_{s,i}|}{n} \quad (12)$$

260 where,  $n$  is the total number of observations. Subscripts of  $o$  and  $s$  refer to observed and simulated  
261 variables, respectively.  $\overline{Q_o}$  is the average value of observed streamflow during the assessing period.

262 An automatic procedure based on the pySOT optimization algorithm developed by Eriksson et al.  
263 (2015) was implemented for all the three calibration variants to identify the behavioral parameters.  
264 pySOT used surrogate model to guide the search for improved solutions, with the advantage of requiring  
265 few function evaluations to find a good solution. An event-driven framework POAP were used for  
266 building and combining asynchronous optimization strategies. The optimization was stopped if a  
267 maximum number of allowed function evaluations was reached, which was set as 3000 in this study. For  
268 the single-, dual- and triple-objective calibration variants,  $NSE_{dis}$ ,  $NSE_{dis} - MAE_{SCA}$ ,  $NSE_{dis} - MAE_{SCA} -$   
269  $MAE_{iso}$  were chosen as combined optimization objectives, respectively. The pySOT algorithm was  
270 repeated 150 times for each calibration variant. The 150 final results were further filtered according to  
271 the metric of  $NSE_{dis}$ , i.e., only the parameters producing  $NSE_{dis}$  higher than a threshold were regarded as  
272 behavioral parameter sets. For single- and dual-objective calibration, the threshold was selected as 0.75.  
273 Considering the trade-off between discharge and isotope simulation, the threshold was chosen as 0.70  
274 for triple-objective calibration. For each calibration variant, the parameter producing highest combined  
275 optimization objective was regarded as the best parameter set.

276 [Table 2]

### 277 2.3 Quantifications of the contributions of runoff components to streamflow

278 The contributions of individual runoff components to streamflow were quantified based on two  
279 definitions of the runoff components. In the first definition, we quantified the contributions of individual  
280 water sources including rainfall, snow meltwater and glacier meltwater to the total water input, which  
281 were commonly reported in previous quantifications of runoff components on the Tibetan Plateau (Chen





282 et al., 2017; Zhang et al., 2013). To be noted, the sum of the three water sources should be larger than the  
283 simulated volume of runoff because of the evaporation loss. Thus, contributions quantified in this  
284 definition only refer to the fractions of the water sources in the total water input forcing runoff processes,  
285 rather than the actual contributions of water sources to streamflow at the basin outlet. In the second  
286 definition, runoff components were quantified based on the runoff generation processes including surface  
287 runoff and subsurface flow. Surface runoff consists of runoff triggered by rainfall and meltwater that feed  
288 streamflow through surface paths, and the precipitation occurring in river channel and contributes to  
289 runoff directly. Subsurface flow is the interflow from groundwater outflow.

#### 290 2.4 Estimation of the water travel time and residence time

291 In this study, the water travel time is estimated by three methods, a lumped analytical method and  
292 two distributed model-based methods. A simplified lumped method, sine-wave method (SW) was used  
293 to provide a reference value of mean travel time (MTT) and mean residence time (MRT) in the catchment.  
294 The adopted model-based methods were developed by van Huijgevoort et al. (2016) and Remondi et al.  
295 (2018), which were referred to as mass-mixing method (MM) and flux-tracking method (FT),  
296 respectively. SW method is based on the isotope data of precipitation and stream water. MM and FT  
297 methods were conducted by the tracer-aided hydrological model using behavior parameter values  
298 identified by the calibration scenarios.

299 SW method has a stationarity assumption that a constant flow field gives constant travel time  
300 distribution (TTDs) (van der Velde et al., 2015). It assumes the form of TTD, and derives the MTT  
301 directly from the series isotopic data (McGuire and McDonnell, 2006). Although the assumption is rather  
302 stringent, SW is widely used in the studies when an approximate estimation of MTT is required (e.g.,  
303 Kirchner, 2016; Garvelmann et al., 2017). Here we assumed the form of TTD as the exponential function,  
304 and the MTT can be estimated according to Eqs. 13-14 (McGuire and McDonnell, 2006; Garvelmann et  
305 al., 2017):

$$306 \quad \delta_t = \bar{\delta} + A * \sin\left(\frac{2\pi}{365} * t + \varphi\right) \quad (13)$$

$$307 \quad MTT = \frac{\sqrt{\left(\frac{1}{A_r/A_p}\right)^2 - 1}}{2\pi} \quad (14)$$

308 where,  $\delta_t$  is the calculated  $\delta^{18}\text{O}$  of stream water or precipitation on day  $t$  of the year.  $\bar{\delta}$  is the mean  $\delta^{18}\text{O}$   
309 of stream water or precipitation measured in different seasons.  $A$  and  $\varphi$  are parameters controlling the  
310 amplitude and phase lag, and are estimated based on the fitness between the sine-wave curve and the  
311  $\delta^{18}\text{O}$  measurements. Subscripts of  $r$  and  $p$  in Eq. 14 represent river and precipitation, respectively.

312 MM method was used to estimate the water age of outflow and water storage in the catchment. For  
313 the outflow (e.g., stream water, evaporation), the concept of water age is consistent with the concept of  
314 “travel time conditional on exit time” by Botter et al. (2011), “flux age” by Hrachowitz et al. (2013), and  
315 “backward travel time” by Harman and Kim (2014). For the water storage (e.g., soil water, groundwater,  
316 snowpack), the concept of water age is consistent with the concept of “residence time” by Botter et al.  
317 (2011) and “residence age” by Hrachowitz et al. (2013). MM method regarded the water age as a kind  
318 of tracer, and simulated the “concentration” of this tracer of the water bodies including snowpack, soil  
319 water and stream water (van Huijgevoort et al., 2016; Ala-aho et al., 2017). The “mass” and



320 “concentration” of the water age were simulated similarly in Eqs. 8-9, by replacing  $\delta^{18}\text{O}$  with water age  
321 of the multiple terms. Event precipitation entering the catchment was treated as new water with a  
322 youngest age equaling to the simulation step of model. The glacier meltwater was regarded as very old  
323 water, and a constant age of 1000 days was adapted in this study. Meanwhile, the age of water stored in  
324 snowpack, soil and river channel were assumed to increase with the ongoing simulation time: water age  
325 increased by one day after each model running at a daily step.

326 FT method ran the model multiple times in parallel to track the fate of each precipitation event  
327 separately (Remondi et al., 2018). All days with precipitation were individually labeled and tracked over  
328 the simulation period by adding an artificial tracer to the water amounts which was assumed to not  
329 otherwise exist anywhere. The snow meltwater was tracked from the time when the snow entered the  
330 catchment as solid precipitation (i.e., snowfall), rather than the time when the snowpack melted. Glacier  
331 meltwater was not tracked, because the evolution of glacier was not simulated in the model, and the travel  
332 time of glacier melt as surface runoff was negligible. Similar as MM method, the MTT of glacier melt  
333 runoff was assumed as a constant value as 1000 days. The mixing and transport processes of the tracer  
334 were also simulated similarly in Eqs 8-9 by replacing  $\delta^{18}\text{O}$  with the concentration of the artificial tracer.  
335 By summarizing the mass of labeled precipitation in the water storage and stream water, the TTD  
336 conditional on exit time (backward TTD), TTD conditional on injection time (forward TTD) and  
337 residence time distribution (RTD) can be derived.

338 In summary, this study estimated the water travel time and residence time using a lumped method  
339 (SW), and two model-based methods (MM and FT), and the results of three methods were compared to  
340 test the robustness of travel time estimation in this glacierized basin. Specifically, SW method estimated  
341 the MTT of total discharge and the MRT of water storage directly based on the isotopic data in stream  
342 water and precipitation. MM method estimated the water age of stream water and groundwater storage,  
343 representing the daily backward MTT and MRT respectively, and all the 19 behavioral parameter sets of  
344 triple-objective calibration were used to illustrate the uncertainty of MTT. FT method estimated the time-  
345 varying precipitation-triggered TTD and RTD, only using the parameter set producing best metric. To  
346 make the result of FT method comparable to MM method, the glacier melt runoff was also assumed to  
347 have MTT (water age) of 1000 days to calculate the MTT of the total runoff generation as the weighted  
348 average value of the MTT of precipitation runoff (including rainfall and snowmelt) and glacier melt  
349 runoff according to the contribution of water sources. The glacier melt was assumed to only contribute  
350 to surface runoff directly and exit the catchment rapidly, thus had no influence on the MRT estimation.

### 351 **3. Results**

#### 352 **3.1 Model performance on the simulations of discharge and isotopic composition**

353 For the calibration period, the single-objective calibration produced good performance for the  
354 simulation of discharge, but had an extremely poor performance for the simulations of SCA and  $\delta^{18}\text{O}$   
355 (Table 3). Involving SCA in the calibration objective, the dual-objective calibration significantly  
356 improved the simulation of SCA, and kept a good behavior on discharge simulation, but brought no  
357 benefit to the isotope simulation. The triple-objective variant led to a good performance for all the three  
358 metrics. The  $\text{NSE}_{\text{dis}}$  produced by triple-objective calibration was slightly lower than that of another two  
359 variants because of the lower threshold for behavior parameter sets. The simulation of isotopic  
360 composition of stream water was significantly improved by triple-objective calibration compared to the  
361 other two variants. For the validation period, the  $\text{NSE}_{\text{dis}}$  of triple-objective calibration was significantly



362 improved, even better than the single-objective, indicating the improved process representation of the  
363 behavior parameters by the triple-objective calibration. Through 150 runs of calibration program, triple-  
364 objective calibration got the smallest behavior parameter sets, indicating that involving additional  
365 calibration objectives increase the identifiability of model parameters and reduce the equifinality.

366 **[Table 3]**

367 Fig. 2 shows the uncertainty ranges of the simulations for the behavioral parameters obtained by  
368 the three calibration variants. The three variants generally produced similar hydrographs in terms of the  
369 magnitudes and timing of peak flows with averaged behavioral parameter sets, but the triple-objective  
370 had a narrower uncertainty range, especially for the baseflow dominated periods (Figs. 2a-c). The single-  
371 objective variant resulted in rather large uncertainty ranges for the simulations of SCA and isotopic  
372 composition (Figs. 2d and g). The good fitness between the simulated and observed streamflow in  
373 summer is likely due to the largely overestimated rainfall-triggered surface runoff, because of the  
374 underestimated reduction of SCA in spring. The dual-objective calibration significantly reduced the  
375 uncertainty range of the SCA simulation, and captured the declining SCA in summer very well (Fig. 2e).  
376 Including SCA in the model calibration, however, only provided small benefits for the simulation of  $\delta^{18}\text{O}$   
377 in stream water (Fig. 2h). Simulations of the triple-objective variant properly reproduced the temporal  
378 variation in SCA in the melt season, despite the slightly reduced performance compared to that of the  
379 dual-objective variant (behaving as higher MAE<sub>SCA</sub> of triple-objective calibration in Table 3). Meanwhile,  
380 the seasonal variations of  $\delta^{18}\text{O}$  of stream water were reproduced well by the triple-objective calibration  
381 (Fig. 2i).

382 **[Figure 2]**

383 Fig. 3a shows median value of the simulated daily inputs of water sources (rainfall, snowmelt, and  
384 glacier melt) for the calibration period obtained by the behavioral parameter sets of the triple-objective  
385 variant. All the three water sources started to contribute to stream water in around April. The volume of  
386 snowmelt peaked around June, and then decreased rapidly in July as the catchment SCA decreased  
387 significantly. The volumes of rainfall and glacier melt peaked in mid-summer which was the wettest and  
388 warmest period in the year. The fluctuations of the simulated  $\delta^{18}\text{O}$  of stream water in Fig. 3b are generally  
389 consistent with the varying contributions of these water sources to runoff. At the beginning of the wet  
390 season,  $\delta^{18}\text{O}$  of stream water increased rapidly in response to the dominance of the isotopic enriched  
391 precipitation. The  $\delta^{18}\text{O}$  of stream water began to decrease in the late wet season, likely because of the  
392 reduced  $\delta^{18}\text{O}$  of precipitation caused by the “temperature effect” (Dansgaard, 1964) and the effect of  
393 southwest monsoon (Yin et al., 2006), as well as the increased contributions of isotopic depleted glacier  
394 melt.

395 **[Figure 3]**

### 396 3.2 Contributions of runoff components

397 The results of runoff component quantification reported in this section were based on the behavioral  
398 parameter sets of the three calibration variants. Table 4 and Figure 4 shows the proportions of water  
399 sources in the mean annual water input during 1<sup>st</sup> January 2007 to 31<sup>st</sup> December 2011. In all the three  
400 calibration variants rainfall provided most of the water quantity for runoff generation (44.2% to 48.0%),  
401 because of the high partition of rainfall (around 347mm) in the annual precipitation (around 587mm).  
402 The single-objective variant estimated the lowest proportion of snowmelt (19.7%), because the the



403 simulation of SCA was not constrained in the calibration, leading to largely overestimated SCA in  
404 comparison to the MODIS SCA estimates due to less melting (Fig. 2d). The dual-objective variant  
405 estimated the highest proportion of glacier melt (33.8%), resulting in a lower proportion of rainfall  
406 (44.2%). Involving the calibration objective of isotope, the triple-objective variant estimated the lowest  
407 proportion of glacier melt (29.2%) by rejecting the parameter sets that produced high contribution of  
408 glacier melt (as shown in Fig. 4), which will be discussed more in detailed in the discussion section. To  
409 be noted, despite above differences, the results of three calibration variant were quite similar, with the  
410 maximum difference lower than 5%. However, the uncertainties of the simulated water proportions  
411 decreased substantially with the increase of data that was involved in the calibration, showing as a  
412 decreasing uncertainty (12.4% to 6.2%, Table 4) and fewer outliers (Fig. 4), demonstrating considerable  
413 values of additional datasets for constraining the simulations of corresponding runoff generation  
414 processes.

415 [Table 4]

416 [Figure 4]

417 Fig. 5 compares the seasonal proportions of water sources in the total water input of the three  
418 calibration variants. The seasonal dominance of the water sources on runoff estimated by the three  
419 calibration variants are similar. In particular, the proportion of rainfall was large (around 55%) in summer  
420 but small in winter when rainfall rarely occurred. Snowmelt and glacier melt dominated the total water  
421 input in winter with proportions of around 60% and 40%, respectively. The proportion of meltwater in  
422 summer was relatively low because of the dominance of rainfall during the summer monsoon. Snowmelt  
423 could only account for around 15% in the total water input in summer because of the significantly reduced  
424 snowpack. The proportion of glacier melt was higher than that of snowmelt in summer because of the  
425 decreasing snow cover area. In the spring months, snowmelt and glacier melt contributed around 55%-  
426 60% and 35%-30% to the total water input, respectively. Rainfall provided the remaining 5%. The glacier  
427 melt provided a steady contribution of around 30%-40% throughout the entire hydrological year. The  
428 seasonal proportions of water sources show slightly different among the calibration variants. Specifically,  
429 the triple-objective calibration estimated not only the highest snowmelt and lowest glacier melt in the  
430 three seasons except winter, but also the highest contribution of rainfall in summer (Fig. 5c). Single-  
431 objective calibration produced the highest contribution of rainfall in autumn, and the highest contribution  
432 snowmelt in winter (Fig. 5a). In addition, the uncertainty ranges of the seasonal proportion during  
433 summer and autumn were obviously reduced by the triple-objective calibration (Fig. 5c).

434 [Figure 5]

435 Table 5 shows the contributions of runoff components to annual runoff. Three calibration variants  
436 resulted in rather similar contributions of surface runoff and subsurface runoff (around 65% and 35%  
437 respectively). Surface runoff was the dominant component in this catchment, because of the large glacier  
438 covered area (around 20%) and the large saturation area (around 20%). The triple-objective calibration  
439 estimated relatively lowest surface runoff (64.9%) and highest subsurface runoff (35.1%). Again, the  
440 triple-objective calibration resulted in lowest uncertainty ranges for the contributions of the runoff  
441 components compared to the other two calibration variants (4.1% compared to 12.1%). Isotope data used  
442 in the triple-objective variant provided additional constraints on the estimation of parameters controlling  
443 the generation of subsurface flow (such as *KKA* and *KKD* in Table 2) and the saturation area where  
444 surface runoff occurred (such as *WM* and *B*), thus constraining the partitioning between surface runoff



445 and subsurface runoff.

446 [Table 5]

### 447 3.3 Estimations of water travel time and residence time

448 The travel time and residence time were estimated for the five water years (2007/1/1 – 2011/12/31)  
449 during the simulation period. The result produced by the best parameter set ( $NSE_{dis} = 0.72$ ,  $MAE_{SCA} =$   
450  $0.079$ ,  $MAE_{iso} = 0.484$ ) was used to test the consistency between the two model-based methods. Based  
451 on the assumption that glacier melt water had an age of 1000 days, the backward MTT and MRT  
452 estimated by MM (FT) method were 1.70 (1.72) and 1.22 (1.17) years, respectively. Fig. 6 shows the  
453 comparison between the results of MM and FT methods. As shown in Fig. 6a and 6d, there were strong  
454 correlation between the daily MTTs (MRTs) estimated by the two methods with a high correlation  
455 coefficient of 0.96 (0.98). The daily MTT and MRT series also showed similar temporal variability  
456 between the two methods as shown in Fig. 6b and 6e. The MRT increased steadily during dry season,  
457 and decreased rapidly during wet season due to the recharge of young precipitation. The daily MTT also  
458 showed steady increasing trend during dry season, but showed significant fluctuation during wet season  
459 because of the combined effect of young precipitation and old glacier meltwater. Fig. 6c and 6e shows  
460 the probability density function of the daily backward MTT and MRT produced by the two methods. The  
461 daily MTT had a large range from 0.42 to 2.75 years, with several peak density values at around 1, 1.5  
462 and 2.67 years, including the influence of the multiple water sources with different ages. On the contrary,  
463 the daily MRT only had a narrow range from 0.75 to 1.75 years, with a significant peak value at around  
464 1.25 years, similar with the MRT. Excluding the effect of glacier meltwater, FT method estimated the  
465 precipitation-triggered backward MTT of runoff as 263 days, significantly smaller than the MRT,  
466 indicating the incomplete mixing in the catchment scale caused by the distributed modelling framework.

467 [Figure 6]

468 The lumped SW method estimated the MTT and MRT as 1.68 years ( $A_r$  and  $A_p$  were estimated as  
469 0.58 and 6.19, respectively). Based on the average result of 19 behavioral parameter sets, the model-  
470 based methods estimated the MTT and MRT as 1.61 and 1.28 respectively. The two kinds of methods  
471 produced similar MTT, indicating the robustness of travel time estimation in this catchment. The  
472 precipitation-triggered MTT (shorter than 1 year) was significantly smaller than the MTT of total runoff  
473 estimated by the lumped method, indicating the effect of old glacier melt water. The glacier melt  
474 contributed to stream water through surface runoff directly, and had no contribution to the water storage,  
475 leading to a smaller model-based MRT compared to MTT. The uncertainty of MTT and MRT estimation  
476 could be reflected by the range produced by MM method by the 19 behavioral parameter sets as shown  
477 in Fig. 7. The standard deviation of the estimated MTT and MRT were 74 and 79 days, respectively. The  
478 uncertainty range during June to August was relatively small (Fig. 7a), indicating that different behavioral  
479 parameters produced similar precipitation-triggered processes during the wet season, and the uncertainty  
480 mainly came from the large range of MRT, i.e., the age of water storage including soil water and  
481 groundwater.

482 [Figure 7]

483 Based on the best parameter set, FT method tracked the transportation of precipitation and produced  
484 time-varying forward TTD, backward TTD and RTD. For simplicity, Fig. 8 shows the average  
485 distributions weighted by the precipitation amount (for forward TTD), runoff generation (for backward



486 TTD) and water storage (for RTD). As shown in Fig. 8a and 8b, the forward and backward TTD were  
487 similar, behaving as a high proportion (~0.3) of the youngest water, which was consistent with the high  
488 proportion of rapid surface runoff. The high proportion of young water led to a similar TTD form as  
489 exponential model. The relative peaks of TTD were mainly around the travel time of integral years,  
490 indicating the influence of baseflow from groundwater, which were recharged by precipitation in the wet  
491 seasons of previous years. The simulated RTD was significantly different from the TTD, behaving as the  
492 low probability density of young water. The young water was mainly recharged by the infiltrating rainfall  
493 and snowmelt, which was negligible compared to the total water storage. Again, the difference between  
494 TTD and RTD indicated the incomplete mixing processes, behaving as affinity for young water due to  
495 the rapid flow pathways such as surface runoff.

496 [Figure 8]

#### 497 4. Discussions

##### 498 4.1 The values of tracer on constraining flow pathways and water storages in the hydrological 499 model

500 This study developed a tracer-aided hydrological model and tested its behavior in a glacierized  
501 catchment. Because of the sampling difficulties on the Tibetan Plateau, the tracer data of the water  
502 sources (e.g., snow, glacier, groundwater) was rather limited compared to other tracer-aided modelling  
503 works (e.g., Ala-aho et al., 2017; He et al., 2019). Nonetheless, the model developed in this study  
504 performed well on producing the tracer signature of stream water, producing a tool for applying the  
505 tracer-aided method to the areas with limited tracer data. Although it was widely accepted that simple  
506 input-output tracer measurements provided limited insight into catchment function, and sampling source  
507 water components would be helpful (Birkel et al., 2014; Tetzlaff et al., 2014), the uncertainty of model  
508 could still be reduced significantly by satisfying the output tracer signature (Delavau et al., 2017),  
509 especially in cold regions where hydrological processes were more complex. The fact that the model can  
510 simultaneously satisfy three calibration objectives over a long period gave confidence in the model  
511 realizations (McDonnell and Beven, 2014).

512 Our results indicate that involving the isotope into calibration significantly reduced the uncertainty  
513 of quantifying the runoff components. To understand the role of isotope data on reducing the uncertainty,  
514 the results of dual-objective calibration variant were analyzed why some of the parameter sets behaved  
515 poorly on isotope simulation despite their good performance on discharge and snow simulation. Among  
516 the 117 behavioral parameter sets of dual-objective calibration, only 14 of them produced relatively good  
517 isotope simulations ( $MAE_{iso} < 1.0$ ). As shown in Fig. 9a and 9b, these 14 isotopic behavioral parameter  
518 sets produced the proportion of runoff component within a relatively smaller range (27.5% to 38% for  
519 glacier melt, and 58% to 75% for surface runoff), while the 117 behavioral parameter sets produced a  
520 much larger variation (24% to 53% for glacier melt, and 40% to 90% for surface runoff). This indicated  
521 that involving isotope data for model calibration helped to exclude some unreasonable proportions of  
522 runoff component. The distribution of scatter in Fig. 9a and Fig. 9b was similar, and the proportion of  
523 surface runoff had a strong correlation with the proportion of glacier melt as shown in Fig. 9c (because  
524 of the assumption that glacier melt contributed to surface runoff directly), thus the mechanism that  
525 isotope can reject unreasonable proportions were the same for water sources and runoff generation  
526 processes. Fig. 9d shows the simulation range of  $\delta^{18}O$  of stream water by calibrated parameters that  
527 resulted in glacier melt proportion in the total water input higher than 40%. The simulated isotopic



signature showed strong fluctuations due to the high proportion of surface runoff with a larger time variation compared to the relatively steady signature of subsurface runoff. Also, the simulated isotopic values were significantly higher than the observations, which was mainly the result of the excessive isotopic fractionation due to the too much evaporation of surface water (Hindshaw et al., 2011; Wolfe et al., 2007). Fig. 9e shows the simulation range by the parameters with proportion of surface runoff lower than 45%. In contrast to scenarios with too high glacier melt, the simulated isotope signature showed small variation and the mean values were much lower than the observation. Our result also showed that the proportion of surface runoff and glacier melt tended to be higher when the  $NSE_{dis}$  was higher, indicating that focusing on the simulation of integrated observation of discharge only will likely lead to overestimated surface runoff and glacier melt. These results indicated that the isotope data helped to constrain the quantifications of runoff components by (1) regulating the competition between rapid component with strong variation of isotope signatures (e.g., surface runoff) and slow component with relatively stable isotope signatures (e.g., subsurface runoff) to match the daily fluctuations of observed isotope signature of stream water, and (2) controlling the isotopic fractionation by adjusting the evaporation to satisfy the observed isotopic value.

[Figure 9]

Two model-based methods (MM and FT) were adopted to estimate travel time and residence time in this study, and verified by the result of lumped method (SW). Both MM and FT methods can estimate MTT and MRT, but FT provided more information including TTD and RTD, which was actually more of interest. MM method has been used in several previous studies, including modelling work in snow-influenced basins (Ala-aho et al., 2017). Consequently, the results of FT and MM were compared in this study, to ensure that the additional information provided by FT method was reasonable. Our result indicated that the two model-based methods produced consistent results, which were also similar with the lumped method, indicating the robustness of MTT and MRT estimation through a tracer-aided model without defining any prior distribution functions.

Although significantly constraining the proportion of runoff component, the uncertainty ranges of simulated MTT and MRT, especially that during baseflow-dominant period (as shown in Fig. 7b) were still rather large, indicating that the estimation of groundwater age had a large uncertainty, which was similar with other model-based age estimation works (e.g., Ala-aho et al., 2017; van Huijgevoort et al., 2016). The isotope observations were mainly collected during wet season when precipitation-triggered surface runoff played an important role in runoff generation, thus this process was constrained relatively well by the isotope calibration, showing as the similar fluctuation of MTT during wet season produced by different parameter sets. Although the proportion of subsurface runoff was constrained, the storage volume of groundwater was poorly constrained, because of the relatively simplified structure of the groundwater module of THREW model (Tian et al., 2006), which adopted a two-layer reservoir model to describe the processes of seepage and subsurface flow. Apart from involving more calibration objectives, improving the physical mechanism and the representation of hydrological processes is another important way to constrain the model behavior and reduce uncertainties.

#### 4.2 Limitation and uncertainty

Multiple water sources brought difficulties to hydrological modelling in glacierized basins (Zongxing et al., 2019). Focusing on the tracer transportation processes, the model developed in this study made some simplifications on the processes related to snow and glacier to make the model structure





570 parsimonious. First, the snow accumulation and melting processes were simulated by a simple  
571 temperature-based method, which was relatively lack of physical mechanism compared to the energy-  
572 based methods (e.g., Pomeroy et al., 2007). Nonetheless, this method had an acceptable behavior and  
573 was widely used in studies of snow simulation (e.g., He et al., 2014), and the simulated SCA was  
574 validated by the MODIS data during ablation period in this study. Second, the evolutions of glacier  
575 thickness and area were not simulated in the model. Simplification of a constant glacier area likely led  
576 to an overestimation of the contribution of glacier melt to runoff, as the glacier cover area should get  
577 smaller due to the climate warming. However, this simplification should have minor influence on the  
578 result because the changes of glacier area was rather small in a short simulation period of seven years.

579 The lack of source water sampling made it difficult to fully validate the modelling result. Although  
580 the isotope signature of stream water was reproduced well, it cannot guarantee that the isotopic variations  
581 of groundwater, snowmelt were simulated correctly. The quantification of runoff components was also  
582 hard to verified. The end-member method cannot be applied as a reference due to the lack of water source  
583 tracer data. A previous study of snow cover and runoff modelling work in the same basin (Zhang et al.,  
584 2015) provided a potential reference. That work indicated that the contribution of rainfall, snowmelt and  
585 glacier melt in 2006 were 30%, 10% and 60%, respectively, which was markedly different from the result  
586 of this study. The runoff simulation in Zhang et al. (2015) was conducted by a simplified conceptual  
587 model with limited physical mechanism, which did not consider the processes of subsurface runoff and  
588 evaporation. And the glacier melt runoff coefficient (the ratio of glacier melt runoff to the total glacier  
589 melt) estimated by that study was very small (0.182), indicating that a large proportion of glacier melt  
590 did not contribute to the surface runoff directly, which is inconsistent with the common assumption in  
591 previous studies (e.g., Seibert et al., 2018; Schaepli et al., 2005). The extremely low glacier melt runoff  
592 coefficient might lead to overestimation of the contribution of glacier melt. The significant differences  
593 between the two studies mainly resulted from the difference of model structure. Intensive source water  
594 sampling together with systematic glacier observation might improve the behavior of hydrological model  
595 in glacierized basins and help us better understand the runoff processes.

596 In glacierized basins where glacier meltwater played an important role on runoff generation, the  
597 object of the three MTT estimation methods were different. The total runoff could be divided into  
598 precipitation-triggered runoff (including rainfall-runoff and snowfall-snowmelt-runoff) and glacier melt  
599 runoff. Considering that glacier was also formed by the precipitation over past years, the lumped SW  
600 method should have reflected both runoff processes, because it was based on the tracer data of  
601 precipitation and total runoff. The two model-based methods mainly focused on the precipitation-  
602 triggered runoff, because the glacier revolution process was simplified in the model. The MTT estimation  
603 of total runoff should be based on the assumed MTT of glacier melt water. In this study, assuming the  
604 MTT of glacier melt as 1000 days, the model-based results were similar with SW method, indicating that  
605 the assumption of glacier melt MTT was appropriate, which was actually misleading. The time scale of  
606 glacier update was much longer than this assumed value, because glacier generally took decades to  
607 hundreds of years to move from accumulation zone to ablation zone (Soncini et al., 2014; Yao et al.,  
608 2012). The good agreement among the three methods indicate that the SW method significantly  
609 underestimated the age of glacier. This was mainly due to the limited applicable time scale of stable  
610 isotope in water. It was reported that seasonal cycle of stable isotope in precipitation were most useful  
611 for inferring relatively short travel time of 2-4 years (McGuire and McDonnell, 2006; Sprenger et al.,  
612 2019; Stewart et al., 2010). The assumed glacier melt MTT of 1000 days was within this range, thus the  
613 similar result of three methods could verify the model representation of the precipitation-triggered runoff





614 process, and the cross validation between MM and FT methods further enhanced the robustness of the  
615 travel time estimation. Consequently, we can expect that if a tracer suitable for longer travel time (e.g.,  
616  $^{14}\text{C}$ ) was used to estimate the proper MTT of total runoff, we could better infer the age of water according  
617 to the model-based estimation of precipitation-triggered runoff MTT.

## 618 5. Conclusions

619 A tracer module was integrated into the THREW hydrological model to constrain the various runoff  
620 processes, and was tested in a glacierized catchment on the Tibetan Plateau. Measurements of oxygen  
621 stable isotopes of the stream water were used to calibrate the model parameters, in addition to the  
622 observations of discharge and MODIS SCA. The behaviors of the model, especially the quantifications  
623 of runoff components were compared among the calibration variants with different objective, to test the  
624 value of isotope data on constraining the model parameters. A lumped method (SW) and two model-  
625 based methods (MM and FT) were applied to estimate the water travel time in the study basin. Our main  
626 findings are:

627 (1) The THREW-t model performed well on simultaneously reproducing the variations of discharge,  
628 snow cover area, and the isotopic composition of stream water, despite of a small water sample number  
629 of precipitation was available to provide isotope input data.

630 (2) The contributions of rainfall, snowmelt and glacier melt to the annual runoff were quantified as  
631 47.4%, 23.4% and 29.2%. Surface runoff (contributing around 64.9%) was more dominant than  
632 subsurface flow in the annual runoff. Calibration with isotope data significantly reduced the uncertainties  
633 by regulating the competition between rapid and slow runoff components to fit the variation of observed  
634 isotope signature, and resulted in more plausible quantifications of contributions of runoff components  
635 to seasonal runoff.

636 (3) The estimated MTT of model-based methods MM and FT met well with that of a sin-wave  
637 lumped parameter method, indicating the robustness of travel time estimation benefiting from the use of  
638 water isotope data. The precipitation-triggered MTT was significantly shorter than the MTT of total  
639 runoff, indicating the effect of old glacier meltwater. The MRT was longer than precipitation-triggered  
640 MTT, indicating the catchment scale incomplete mixing processes, and the affinity for young water due  
641 to the rapid flow pathways such as runoff on impermeable glacier surface.

## 642 Code/Data availability

643 The isotope data and the code of THREW-t model used in this study are available by contacting the  
644 authors.

## 645 Author contribution

646 YN, ZH and FT conceived the idea; LT provided the observation data; FT provided financial support;  
647 YN and conducted analysis; LT and LS provided comments on the analysis; all the authors contributed  
648 to writing and revisions.

## 649 Competing interests

650 The authors declare that they have no conflict of interest.



651 **Acknowledgements**

652 This study was supported by the National Science Foundation of China (92047301, 91647205). The  
653 authors would like to thank Kunbiao Li from Tsinghua University for the contribution of the coding of  
654 calibration program. The authors thank all the organizations and scientists for the contribution of data  
655 used in this work. Datasets of glacier, snow cover and vegetation for this study are available in these in-  
656 text data citation referees: Liu (2012), Hall and Riggs (2016), Didan (2015) and Myneni et al. (2015).  
657 The digital elevation model (DEM) data set is available at Geospatial Data Cloud site, Computer Network  
658 Information Center, Chinese Academy of Sciences (<http://www.gsccloud.cn>). The meteorological data is  
659 available at China Meteorological Data System (<http://data.cma.cn>). The soil data is available at the Food  
660 and Agriculture Organization of the United Nations (<http://www.fao.org/geonetwork/>). All the data used  
661 in this study will be available at the Zenodo website at the time of publication or on request from the  
662 corresponding author (tianfq@mail.tsinghua.edu.cn).

663 **Financial support**

664 This study was supported by the National Science Foundation of China (grant no. 92047301, 91647205).

665 **References**

- 666 Ala-Aho, P. , Tetzlaff, D. , Mcnamara, J. P. , Laudon, H. , & Soulsby, C. . (2017). Using isotopes to  
667 constrain water flux and age estimates in snow-influenced catchments using the starr (spatially  
668 distributed tracer-aided rainfall–runoff) model. *Hydrology and Earth System Sciences*  
669 *Discussions*, 21(10), 5089-5110.
- 670 Benettin, P., & Bertuzzo, E. (2018). tran-SAS v1. 0: a numerical model to compute catchment-scale  
671 hydrologic transport using StorAge Selection functions. *Geoscientific Model Development*, 11(4),  
672 1627-1639.
- 673 Birkel, C. , Soulsby, C. , & Tetzlaff, D. . (2014). Developing a consistent process-based conceptualization  
674 of catchment functioning using measurements of internal state variables. *Water Resources Research*,  
675 50(4), 3481–3501.
- 676 Birkel, C., Tetzlaff, D., Dunn, S. M., & Soulsby, C. (2011). Using time domain and geographic source  
677 tracers to conceptualize streamflow generation processes in lumped rainfall-runoff models. *Water*  
678 *Resources Research*, 47(2).
- 679 Botter, G. , Bertuzzo, E. , & Rinaldo, A. . (2011). Catchment residence and travel time distributions: the  
680 master equation. *Geophysical Research Letters*, 38(11).
- 681 Capell, R., Tetzlaff, D., & Soulsby, C. (2012). Can time domain and source area tracers reduce uncertainty  
682 in rainfall-runoff models in larger heterogeneous catchments?. *Water Resources Research*, 48(9).
- 683 Chen, X. , Long, D. , Hong, Y. , Zeng, C. , & Yan, D. . (2017). Improved modeling of snow and glacier  
684 melting by a progressive two-stage calibration strategy with grace and multisource data: how snow  
685 and glacier meltwater contributes to the runoff of the upper brahmaputra river basin?. *Water resources*  
686 *research*, 53(3), 2431-2466.



- 687 Dansgaard, W. (1964). Stable isotopes in precipitation. *Tellus*, 16(4), 436-468.
- 688 Delavau, C. J., Stadnyk, T., & Holmes, T. (2017). Examining the impacts of precipitation isotope input  
689 ( $\delta^{18}\text{O}_{\text{ppt}}$ ) on distributed, tracer-aided hydrological modelling. *Hydrology and Earth System*  
690 *Sciences*, 21(5), 2595-2614.
- 691 Didan, K. (2015). MOD13A3 MODIS/Terra vegetation Indices Monthly L3 Global 1km SIN Grid V006  
692 [Data set]. NASA EOSDIS Land Processes DAAC. Accessed 2020-01-01 from  
693 <https://doi.org/10.5067/MODIS/MOD13A3.006>
- 694 Dou, Y., Chen, X., Bao, A., & Li, L. (2011). The simulation of snowmelt runoff in the ungauged kaidu  
695 river basin of tianshan mountains, china. *Environmental Earth Sciences*, 62(5), 1039-1045.
- 696 Duethmann, D., Bolch, T., Farinotti, D., Kriegel, D., Vorogushyn, S., Merz, B., ... & Güntner, A. (2015).  
697 Attribution of streamflow trends in snow and glacier melt-dominated catchments of the Tarim River,  
698 Central Asia. *Water Resources Research*, 51(6), 4727-4750.
- 699 Duethmann, D., Peters, J., Blume, T., Vorogushyn, S., & Güntner, A. (2014). The value of satellite-  
700 derived snow cover images for calibrating a hydrological model in snow-dominated catchments in  
701 Central Asia. *Water resources research*, 50(3), 2002-2021.
- 702 Eriksson, D., Bindel, D., & Shoemaker, C. (2015). Surrogate optimization toolbox (pysot).
- 703 Finger, D., Vis, M., Huss, M., & Seibert, J. (2015). The value of multiple data set calibration versus  
704 model complexity for improving the performance of hydrological models in mountain  
705 catchments. *Water resources research*, 51(4), 1939-1958.
- 706 Gao J., Tian L., & Liu Y. (2009). Oxygen isotope variation in the water cycle of the Yamdrok-tso Lake  
707 Basin in southern Tibetan Plateau. *Chinese Sci Bull*, 54: 2758—2765
- 708 Garvelmann, Jakob, Warscher, Michael, Leonhardt, Gabriele, Franz, Helmut, Lotz, Annette, &  
709 Kunstmann, Harald. (2017). Quantification and characterization of the dynamics of spring and stream  
710 water systems in the berchtesgaden alps with a long-term stable isotope dataset. *Environmental Earth*  
711 *Sciences*, 76(22), 766.
- 712 Hall, D. K. and G. A. Riggs. (2016). MODIS/Terra Snow Cover 8-Day L3 Global 500m SIN Grid,  
713 Version 6. [Data set]. Boulder, Colorado USA. NASA National Snow and Ice Data Center Distributed  
714 Active Archive Center. Accessed 2020-01-01 from <https://doi.org/10.5067/MODIS/MOD10A2.006>.
- 715 Harman, C. J. (2019). Age - ranked storage - discharge relations: a unified description of spatially  
716 lumped flow and water age in hydrologic systems. *Water Resources Research*, 55(8).
- 717 He, Z. H., Parajka, J., Tian, F. Q., & Blöschl, G. (2014). Estimating degree day factors from MODIS for  
718 snowmelt runoff modeling. *Hydrology & Earth System Sciences Discussions*, 11(7).
- 719 He, Z. H., Tian, F. Q., Gupta, H. V., Hu, H. C., & Hu, H. P. (2015). Diagnostic calibration of a hydrological  
720 model in a mountain area by hydrograph partitioning. *Hydrology and Earth System Sciences*, 19(4),



- 721 1807.
- 722 He, Z. , Vorogushyn, S. , Unger-Shayesteh, K. , Gafurov, A. , Kalashnikova, O. , & Omorova, E. , et al.  
723 (2018). The value of hydrograph partitioning curves for calibrating hydrological models in glacierized  
724 basins. *Water Resources Research*, 54(3), 2336-2361.
- 725 He, Z. , Unger-Shayesteh, K. , Vorogushyn, S. , Weise, S. M. , Kalashnikova, O. , & Gafurov, A. , et al.  
726 (2019). Constraining hydrological model parameters using water isotopic compositions in a  
727 glacierized basin, central asia. *Journal of Hydrology*.
- 728 He, Z., Unger-Shayesteh, K., Vorogushyn, S., Weise, S., Duethmann, D., Kalashnikova, O., Gafurov, A.,  
729 Merz, B., 2020. Comparing Bayesian and traditional end-member mixing approaches for hydrograph  
730 separation in a glacierized basin. *Hydrol. Earth Syst. Sci. Hydrol. Earth Syst. Sci.*, 24, 3289–3309,  
731 <https://doi.org/10.5194/hess-24-3289-2020>
- 732 Hindshaw, R. S., Tipper, E. T., Reynolds, B. C., Lemarchand, E., Wiederhold, J. G., Magnusson, J., ... &  
733 Bourdon, B. (2011). Hydrological control of stream water chemistry in a glacial catchment (Damma  
734 Glacier, Switzerland). *Chemical Geology*, 285(1-4), 215-230.
- 735 Hrachowitz, M. , Savenije, H. , Bogaard, T. A. , Tetzlaff, D. , & Soulsby, C. . (2013). What can flux  
736 tracking teach us about water age distribution patterns and their temporal dynamics?. *Hydrology and*  
737 *Earth System Sciences*, 17(2), 533-564.
- 738 Immerzeel, W.W., Pellicciotti, F., Bierkens, M.F.P., 2013. Rising river flows throughout the twenty-first  
739 century in two Himalayan glacierized watersheds. *Nat. Geosci.* 6, 742–745.  
740 <https://doi.org/10.1038/ngeo1896>
- 741 Immerzeel, W. W., Van Beek, L. P., & Bierkens, M. F. (2010). Climate change will affect the Asian water  
742 towers. *Science*, 328(5984), 1382-1385.
- 743 Kirchner, J. W. (2016). Aggregation in environmental systems - part 1: seasonal tracer cycles quantify  
744 young water fractions, but not mean transit times, in spatially heterogeneous catchments. *Hydrology*  
745 *& Earth System Sciences*.
- 746 Kong, Y., Pang, Z., 2012. Evaluating the sensitivity of glacier rivers to climate change based on  
747 hydrograph separation of discharge. *J. Hydrol.* 434–435, 121–129.  
748 <https://doi.org/10.1016/j.jhydrol.2012.02.029>
- 749 Konz, M., & Seibert, J. (2010). On the value of glacier mass balances for hydrological model  
750 calibration. *Journal of hydrology*, 385(1-4), 238-246.
- 751 Kumar, R. , Singh, S. , Kumar, R. , Singh, A. , Bhardwaj, A. , & Sam, L. , et al. (2016). Development of  
752 a glacio-hydrological model for discharge and mass balance reconstruction. *Water Resources*  
753 *Management*, 30(10), 3475-3492.
- 754 Liu, Z., Tian, L., Yao, T., Gong, T., Yin, C., & Yu, W. (2007). Temporal and spatial variations of  $\delta^{18}O$   
755 in precipitation of the Yarlung Zangbo River Basin. *Journal of Geographical Sciences*, 17(3), 317-



- 756 326.
- 757 Liu S. (2012). The second glacier inventory dataset of China (version 1.0) (2006-2011) [Data set].  
758 National Tibetan Plateau Data Center. Accessed 2020-01-01 from  
759 <https://doi.org/10.3972/glacier.001.2013.db>.
- 760 Luo, Y. , Wang, X. , Piao, S. , Sun, L. , Ciais, P. , & Zhang, Y. , et al. (2018). Contrasting streamflow  
761 regimes induced by melting glaciers across the tien shan – pamir – north karakoram. *Scientific*  
762 *Reports*, 8(1).
- 763 Lutz, A. F. , Immerzeel, W. W. , Shrestha, A. B. , & Bierkens, M. F. P. . (2014). Consistent increase in  
764 high asia's runoff due to increasing glacier melt and precipitation. *Nature Climate Change*.
- 765 Lutz, A.F., Immerzeel, W.W., Kraaijenbrink, P.D.A., Shrestha, A.B., Bierkens, M.F.P., 2016. Climate  
766 Change Impacts on the Upper Indus Hydrology: Sources , Shifts and Extremes 1–33.  
767 <https://doi.org/10.1371/journal.pone.0165630>
- 768 Marques, J. E. , Samper, J. , Pisani, B. , Alvares, D. , Carvalho, J. M. , & H. I. Chaminé, et al. (2011).  
769 Evaluation of water resources in a high-mountain basin in serra da estrela, central portugal, using a  
770 semi-distributed hydrological model. *Environmental Earth Sciences*, 62(6), 1219-1234.
- 771 McDonnell, J. J., & Beven, K. (2014). Debates—The future of hydrological sciences: A (common) path  
772 forward? A call to action aimed at understanding velocities, celerities and residence time distributions  
773 of the headwater hydrograph. *Water Resources Research*, 50(6), 5342-5350.
- 774 McGuire, K. J. , & McDonnell, J. J. . (2006). A review and evaluation of catchment transit time  
775 modeling. *Journal of Hydrology*, 330(3-4), 0-563.
- 776 McMillan, H., Tetzlaff, D., Clark, M., Soulsby, C., 2012. Do time-variable tracers aid the evaluation of  
777 hydrological model structure? A multimodel approach. *Water Resour. Res.* 48.  
778 <https://doi.org/10.1029/2011WR011688>
- 779 Miller, J. D., Immerzeel, W. W., & Rees, G. (2012). Climate change impacts on glacier hydrology and  
780 river discharge in the Hindu Kush–Himalayas. *Mountain Research and Development*, 32(4), 461-467.
- 781 Myneni, R., Knyazikhin, Y., Park, T. (2015). MOD15A2H MODIS/Terra Leaf Area Index/FPAR 8-Day  
782 L4 Global 500m SIN Grid V006 [Data set]. NASA EOSDIS Land Processes DAAC. Accessed 2020-  
783 01-01 from <https://doi.org/10.5067/MODIS/MOD15A2H.006>
- 784 Mi, D., Xie, Z., & Luo, R. (2001). China Glacier Information System XI: Gangze Water System.
- 785 Nash, J. E., & Sutcliffe, J. V. (1970). River flow forecasting through conceptual models part I—A  
786 discussion of principles. *Journal of hydrology*, 10(3), 282-290.
- 787 Nepal, S. , Chen, J. , Penton, D. J. , Neumann, L. E. , Zheng, H. , & Wahid, S. . (2017). Spatial gr4j  
788 conceptualization of the tamor glaciated alpine catchment in eastern nepal: evaluation of gr4jsg  
789 against streamflow and modis snow extent. *Hydrological Processes*, 31(1), 51-68.



- 790 Nepal, S., Krause, P., Flügel, W., Fink, M., Fischer, C., 2014. Understanding the hydrological system  
791 dynamics of a glaciated alpine catchment in the Himalayan region using the J2000 hydrological model.  
792 *Hydrol. Process.*, 28, 1329–1344. <https://doi.org/10.1002/hyp.9627>
- 793 Nepal, S., Zheng, H., Penton, D. J., Neumann, L. E., 2015. Comparative performance of GR4JSG and  
794 J2000 hydrological models in the Dudh Koshi catchment of the Himalayan region. In *MODSIM2015,*  
795 *21st International Congress on Modelling and Simulation*, Weber T, McPhee MJ, Anderssen RS (eds).  
796 Modelling and Simulation Society of Australia and New Zealand: Gold Coast; 2395–2401. ISBN:978-  
797 0-9872143-5-5
- 798 Parajka, J., & Blöschl, G. (2008). The value of modis snow cover data in validating and calibrating  
799 conceptual hydrologic models. *Journal of Hydrology*, 358(3-4), 240-258.
- 800 Pomeroy, J. W., Gray, D. M., Brown, T., Hedstrom, N. R., Quinton, W. L., & Granger, R. J., et al.  
801 (2007). The cold regions hydrological model: a platform for basing process representation and model  
802 structure on physical evidence. *Hydrological Processes*.
- 803 Remondi, F., Kirchner, J. W., Burlando, P., & Faticchi, S. (2018). Water flux tracking with a distributed  
804 hydrological model to quantify controls on the spatiotemporal variability of transit time distributions.  
805 *Water Resources Research*, 54(4), 3081-3099.
- 806 Schaeffli, B., Hingray, B., Niggli, M., & Musy, A. (2005). A conceptual glacio-hydrological model for  
807 high mountainous catchments.
- 808 Schaeffli, B., & Huss, M. (2011). Integrating point glacier mass balance observations into hydrologic  
809 model identification. *Hydrology and Earth System Sciences*, 15(ARTICLE), 1227-1241.
- 810 Seibert, J., Vis, M. J. P., Kohn, I., Weiler, M., & Stahl, K. (2018). Technical note: representing glacier  
811 geometry changes in a semi-distributed hydrological model. *Hydrology & Earth System Sciences*  
812 *Discussions*, 1-20.
- 813 Sivapalan, M., Takeuchi, K., Franks, S. W., Gupta, V. K., Karambiri, H., & Lakshmi, V., et al. (2003).  
814 A decade on predictions in ungauged basins (pub), 2003–2012: shaping an exciting future for the  
815 hydrological sciences. *International Association of Scientific Hydrology Bulletin*, 48(6), 857-880.
- 816 Son, K., & Sivapalan, M. (2007). Improving model structure and reducing parameter uncertainty in  
817 conceptual water balance models through the use of auxiliary data. *Water resources research*, 43(1).
- 818 Soncini, A., Bocchiola, D., Confortola, G., Bianchi, A., & Diolaiuti, G. (2015). Future hydrological  
819 regimes in the upper Indus basin: a case study from a high-altitude glacierized catchment. *Journal of*  
820 *Hydrometeorology*, 16(1), 306-326.
- 821 Soulsby, C., Birkel, C., Geris, J., Dick, J., Tunaley, C., Tetzlaff, D., 2015. Stream water age distributions  
822 controlled by storage dynamics and nonlinear hydrologic connectivity: Modeling with high-resolution  
823 isotope data. *Water Resour. Res.* 5, 2–2. <https://doi.org/10.1111/j.1752-1688.1969.tb04897.x>
- 824 Siderius, C., Biemans, H., Wiltshire, A., Rao, S., Franssen, W. H. P., Kumar, P., Gosain, A. K., Vliet, M.



- 825 T. H. Van, Collins, D. N., 2013. Science of the Total Environment Snowmelt contributions to  
826 discharge of the Ganges. *Sci. Total Environ.* 468–469, S93–S101.  
827 <https://doi.org/10.1016/j.scitotenv.2013.05.084>
- 828 Sprenger, M. , Stumpp, C. , Weiler, M. , Aeschbach, W. , & Werner, C. . (2019). The demographics of  
829 water: a review of water ages in the critical zone. *Reviews of Geophysics*.
- 830 Stadnyk, T. A., & Holmes, T. L. (2020). On the value of isotope-enabled hydrological model  
831 calibration. *Hydrological Sciences Journal*, 1-14.
- 832 Stewart, M. K. , Morgenstern, U. , & McDonnell, J. J. . (2010). Truncation of stream residence time: how  
833 the use of stable isotopes has skewed our concept of streamwater age and origin. *Hydrological*  
834 *Processes*, 24(12), 1646-1659.
- 835 Terzer, S., Wassenaar, L. I., Araguás-Araguás, L. J., & Aggarwal, P. K. (2013). Global isoscapes for  $\delta^{18}\text{O}$   
836 and  $\delta^2\text{H}$  in precipitation: improved prediction using regionalized climatic regression  
837 models. *Hydrology and Earth System Sciences*, 17(11), 4713-4728.
- 838 Tetzlaff, D. , Birkel, C. , Dick, J. , Geris, J. , & Soulsby, C. . (2014). Storage dynamics in hydrogeological  
839 units control hillslope connectivity, runoff generation, and the evolution of catchment transit time  
840 distributions. *Water Resources Research*.
- 841 The newest report from the second scientific expedition to Tibetan Plateau, 2018.  
842 (<http://energy.people.com.cn/n1/2018/0910/c71661-30281998.html>).
- 843 Tian, F., Hu, H., Lei, Z., & Sivapalan, M. (2006). Extension of the Representative Elementary Watershed  
844 approach for cold regions via explicit treatment of energy related processes.
- 845 Tian, F., Li, H., & Sivapalan, M. (2012). Model diagnostic analysis of seasonal switching of runoff  
846 generation mechanisms in the Blue River basin, Oklahoma. *Journal of Hydrology*, 418, 136-149.
- 847 Tian F. , Xu R. , Nan Y. , Li K. , He Z. . (2020) Quantification of runoff components in the Yarlung  
848 Tsangpo River using a distributed hydrological model. *Advances in Water Science*, 31(3): 324-336.
- 849 van der Velde, Y., Heidbüchel, I., Lyon, S. W., Nyberg, L., Rodhe, A., Bishop, K., & Troch, P. A. (2015).  
850 Consequences of mixing assumptions for time - variable travel time distributions. *Hydrological*  
851 *Processes*, 29(16), 3460-3474.
- 852 van Huijgevoort, M. H. J., Tetzlaff, D., Sutanudjaja, E. H., & Soulsby, C. (2016). Using high resolution  
853 tracer data to constrain water storage, flux and age estimates in a spatially distributed rainfall-runoff  
854 model. *Hydrological Processes*, 30(25), 4761-4778.
- 855 Weiler, M., Seibert, J., Stahl, K., 2018. Magic components — why quantifying rain , snowmelt , and  
856 icemelt in river discharge is not easy. *Hydrol. Process.* 32, <https://doi.org/10.1002/hyp.11361>
- 857 Wilusz, D. C., Harman, C. J., & Ball, W. P. (2017). Sensitivity of catchment transit times to rainfall  
858 variability under present and future climates. *Water Resources Research*, 53(12), 10231-10256.



- 859 Wolfe, B. B., Karst-Riddoch, T. L., Hall, R. I., Edwards, T. W., English, M. C., Palmini, R., ... & Vardy,  
860 S. R. (2007). Classification of hydrological regimes of northern floodplain basins (Peace–Athabasca  
861 Delta, Canada) from analysis of stable isotopes ( $\delta^{18}\text{O}$ ,  $\delta^2\text{H}$ ) and water chemistry. *Hydrological  
862 Processes: An International Journal*, 21(2), 151-168.
- 863 Xu, R., Hu, H., Tian, F., Li, C., & Khan, M. Y. A. (2019). Projected climate change impacts on future  
864 streamflow of the Yarlung Tsangpo-Brahmaputra River. *Global and Planetary Change*, 175, 144-159.
- 865 Yang, L., Tian, F., Sun, Y., Yuan, X., & Hu, H. (2014). Attribution of hydrologic forecast uncertainty  
866 within scalable forecast windows. *Hydrology and Earth System Sciences*, 18(2), 775.
- 867 Yao, T., Thompson, L., Yang, W., Yu, W., Gao, Y., & Guo, X., et al. (2012). Different glacier status  
868 with atmospheric circulations in tibetan plateau and surroundings. *Nature Climate Change*, 2.
- 869 Yin, C., Tian, L., Yu W. & Gong T. (2006). Variations of stable oxygen isotope in precipitation in the  
870 Basin of Yamzho Lake. *Journal of Glaciology and Geocryology*, 28(6), 918-924.
- 871 Zhang F., Li J., & Gong T. (2006). Hydrological regime of the Karuxung watershed in north  
872 Himalayas. *Acta Geographica Sinica*, 61(11), 1141-1148.
- 873 Zhang, F., Zhang, H., Hagen, S. C., Ye, M., Wang, D., Gui, D., ... & Liu, J. (2015). Snow cover and runoff  
874 modelling in a high mountain catchment with scarce data: effects of temperature and precipitation  
875 parameters. *Hydrological processes*, 29(1), 52-65.
- 876 Zhang, L., Su, F., Yang, D., Hao, Z., & Tong, K. (2013). Discharge regime and simulation for the  
877 upstream of major rivers over Tibetan Plateau. *Journal of Geophysical Research:  
878 Atmospheres*, 118(15), 8500-8518.
- 879 Zongxing, L., Qi, F., Zongjie, L., Ruifeng, Y., Juan, G., & Yuemin, L. (2019). Climate background,  
880 fact and hydrological effect of multiphase water transformation in cold regions of the western china:  
881 a review. *EARTH ENCE REVIEWS*.
- 882

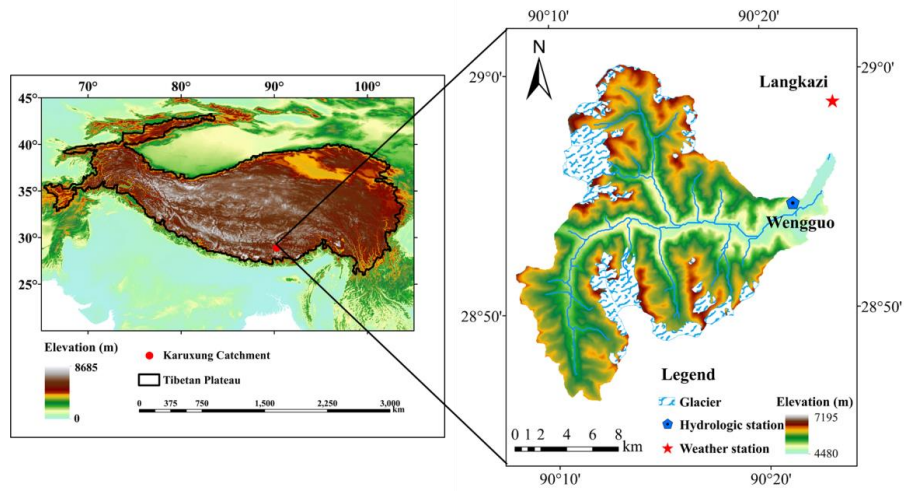




883

#### List of figures

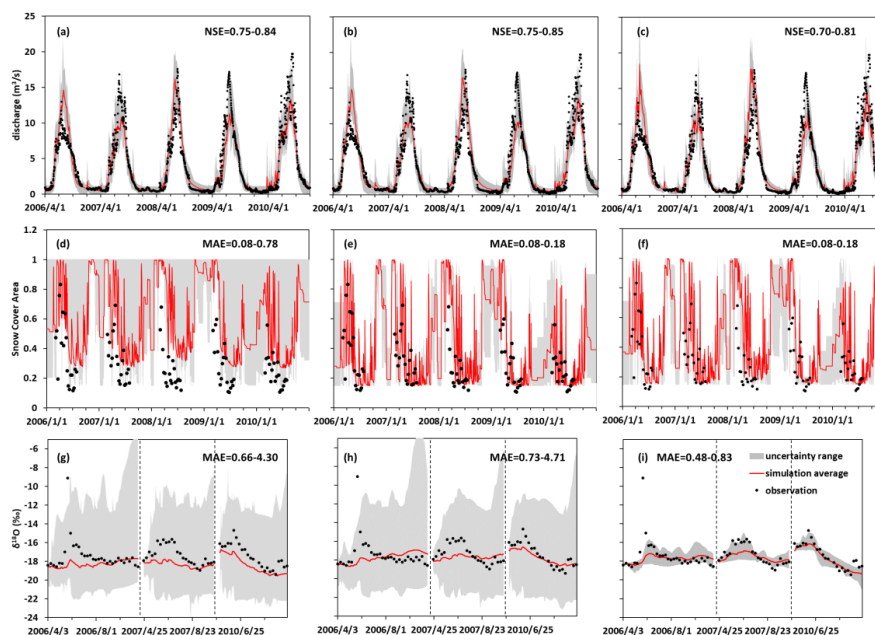
- 884 1. **Figure 1.** Location and topography of the study area
- 885 2. **Figure 2.** Uncertainty ranges of simulations in the calibration period produced by the behavioral  
886 parameter sets of the single-objective (subfigure a to c), dual-objective (subfigure d to f) and triple-  
887 objective (subfigure g to i) calibration variants.
- 888 3. **Figure 3.** Daily simulations of (a) each water source and (b) the corresponding isotopic compositions
- 889 4. **Figure 4.** Average proportion of different sources in the annual water input for runoff generation
- 890 5. **Figure 5.** Seasonal contributions of rainfall, snowmelt and glacier melt to total water input estimated  
891 by the (a) single-objective, (b) dual-objective and (c) triple-objective calibration variants. The error  
892 bars indicate the uncertainty ranges simulated by the corresponding behavior parameter sets.
- 893 6. **Figure 6.** Comparison between the MM and FT methods: scatterplots for daily (a) MTT and (d)  
894 MRT; time series of the daily (b) MTT and (e) MRT; and probability density functions of the daily  
895 (c) MTT and (f) MRT.
- 896 7. **Figure 7.** Uncertainty ranges of time series (a) MTT and (b) MRT simulated by MM method.
- 897 8. **Figure 8.** The weighted average probability distributions of (a) forward TTD, (b) backward TTD,  
898 and (c) RTD estimated by FT method.
- 899 9. **Figure 9.** The role of isotope calibration on constraining the proportion of runoff components. (a)  
900 The relationship between  $MAE_{iso}$  and proportion of glacier melt. (b) The relationship between  
901  $MAE_{iso}$  and proportion of surface runoff. (c) The relationship between proportion of surface runoff  
902 and that of glacier melt. (d) The simulated isotope in stream water produced by the parameter sets  
903 estimating proportion of glacier melt higher than 40%. (e) The simulated isotope in stream water  
904 produced by the parameter sets estimating proportion of surface runoff lower than 45%.  
905



906

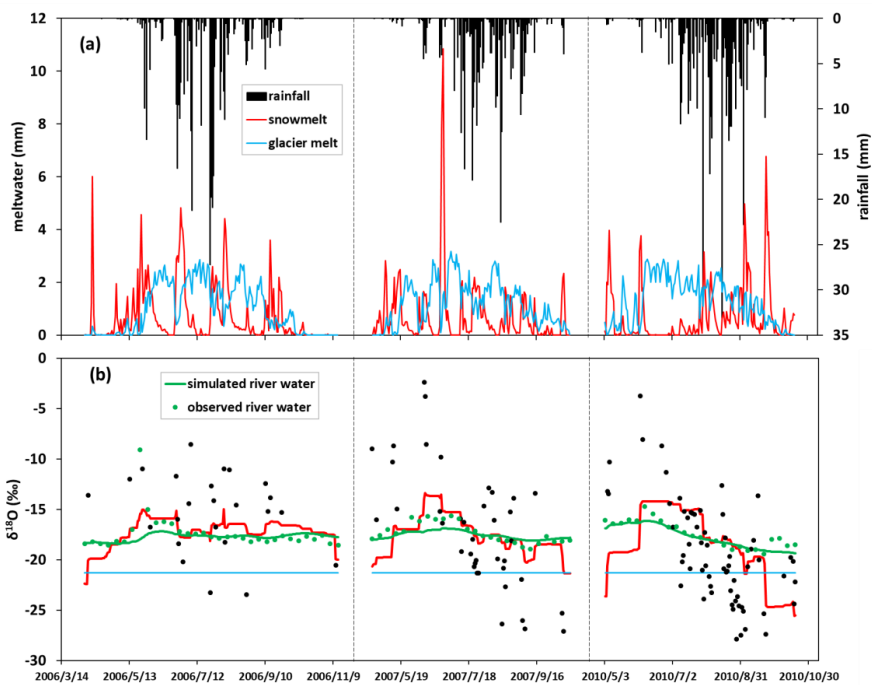
907 **Figure 1.** Location and topography of the study area

908



909

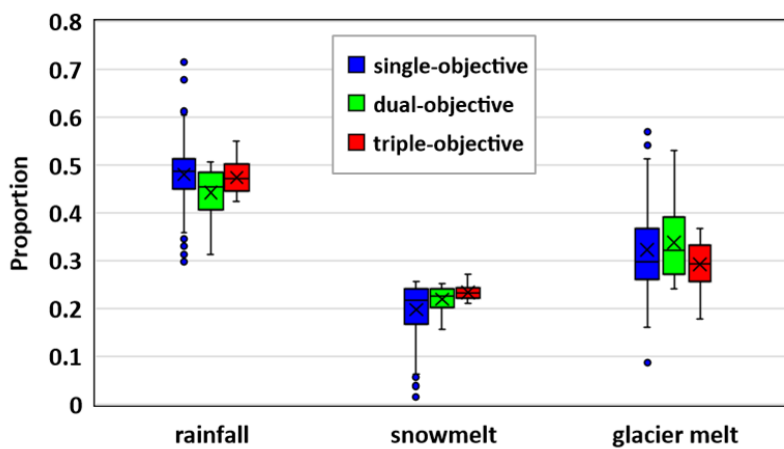
910 **Figure 2.** Uncertainty ranges of simulations in the calibration period produced by the behavioral  
911 parameter sets of the single-objective (subfigure a to c), dual-objective (subfigure d to f) and  
912 triple-objective (subfigure g to i) calibration variants.  
913



914

915 **Figure 3.** Daily simulations of (a) each water source and (b) the corresponding isotopic compositions

916

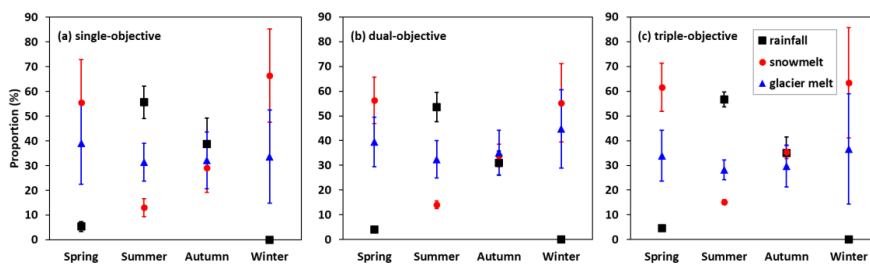


917

918

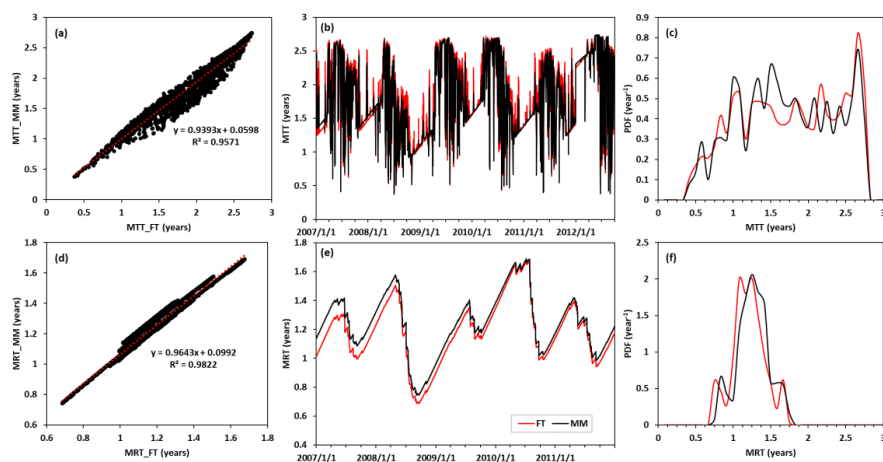
919

**Figure 4.** Average proportion of different sources in the annual water input for runoff generation



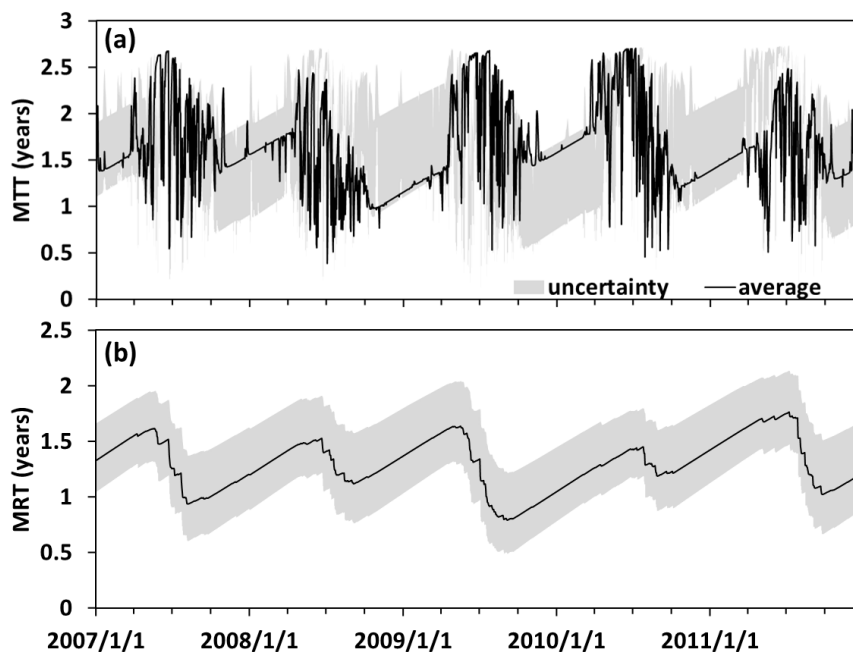
920

921 **Figure 5.** Seasonal contributions of rainfall, snowmelt and glacier melt to total water input estimated by  
922 the (a) single-objective, (b) dual-objective and (c) triple-objective calibration variants. The error bars  
923 indicate the uncertainty ranges simulated by the corresponding behavior parameter sets.  
924



925

926 **Figure 6.** Comparison between the MM and FT methods: scatterplots for daily (a) MTT and (d) MRT;  
927 time series of the daily (b) MTT and (e) MRT; and probability density functions of the daily (c) MTT and  
928 (f) MRT.  
929



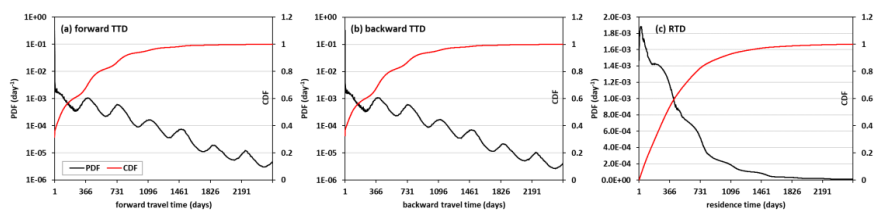
930

931

932

**Figure 7.** Uncertainty ranges of time series (a) MTT and (b) MRT simulated by MM method.

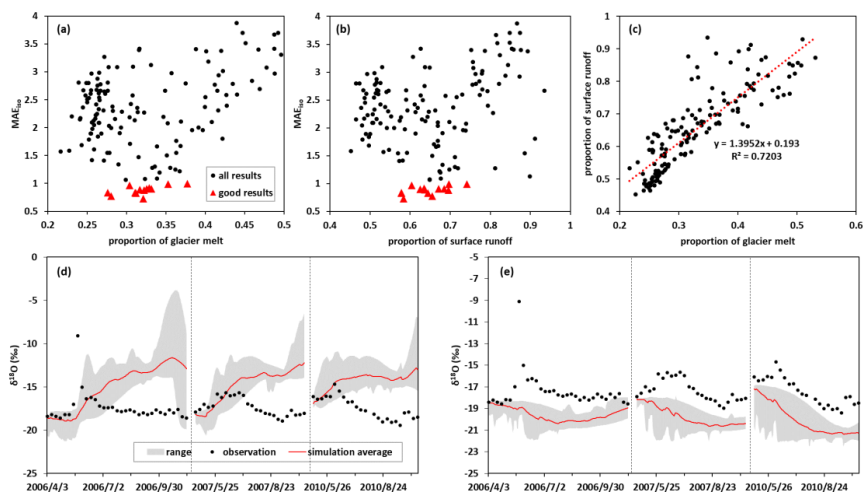




933

934 **Figure 8.** The weighted average probability distributions of (a) forward TTD, (b) backward TTD, and (c)  
935 RTD estimated by FT method

936



937

938 **Figure 9.** The role of isotope calibration on constraining the proportion of runoff components. (a) The  
939 relationship between MAE<sub>18O</sub> and proportion of glacier melt. (b) The relationship between MAE<sub>18O</sub> and  
940 proportion of surface runoff. (c) The relationship between proportion of surface runoff and that of glacier  
941 melt. (d) The simulated isotope in stream water produced by the parameter sets estimating proportion of  
942 glacier melt higher than 40%. (e) The simulated isotope in stream water produced by the parameter sets  
943 estimating proportion of surface runoff lower than 45%.  
944



945	<b>List of tables</b>
946	1. <b>Table 1.</b> Characteristics of the precipitation and stream water samples
947	2. <b>Table 2.</b> Calibrated parameters of the THREW-t model
948	3. <b>Table 3.</b> Comparisons of the model performance produced by three calibration variants.
949	4. <b>Table 4.</b> Average percentages of water sources in the annual water input for runoff generation.
950	5. <b>Table 5.</b> Simulated contributions of runoff components to annual runoff
951	



952 **Table 1.** Characteristics of precipitation and stream samples

Year	Period	Precipitation sample number	Stream sample number
2006	April 6 <sup>th</sup> to November 11 <sup>th</sup>	24	31
2007	April 23 <sup>rd</sup> to October 9 <sup>th</sup>	39	25
2010	May 5 <sup>th</sup> to October 18 <sup>th</sup>	63	23
2011	March 28 <sup>th</sup> to November 6 <sup>th</sup>	69	32
2012	June 16 <sup>th</sup> to September 22 <sup>nd</sup>	42	14

953

954



955 **Table 2.** Calibrated parameters of the THREW-t model

Symbol	Unit	Physical descriptions	Range
$nt$	-	Manning roughness coefficient for hillslope	0-0.2
$WM$	cm	Tension water storage capacity, used in Xinanjiang model (Zhao, 1992) to calculate saturation area	0-10
$B$	-	Shape coefficient used in Xinanjiang model to calculate saturation area	0-1
$KKA$	-	Coefficient to calculate subsurface runoff in $Rg=KKD \cdot S \cdot K_s^S \cdot (y_s/Z)^{KKA}$ , where $S$ is the topographic slope, $K_s^S$ is the saturated hydraulic conductivity, $y_s$ is the depth of saturated groundwater, $Z$ is the total soil depth	0-6
$KKD$	-	See description for $KKA$	0-0.5
$T_0$	°C	Melting threshold temperature used in Eqs. (1) and (2)	-5-5
$DDF_N$	mm/°C/day	Degree day factor for snow	0-10
$DDF_G$	mm/°C/day	Degree day factor for glacier	0-10
$CI$	-	Coefficient to calculate the runoff concentration process using Muskingum method: $O_2=C_1 \cdot I_1+C_2 \cdot I_2+C_3 \cdot O_1+C_4 \cdot Q_{lat}$ , where $I_1$ and $O_1$ is the inflow and outflow at prior step, $I_2$ and $O_2$ is the inflow and outflow at current step, $Q_{lat}$ is lateral flow of the river channel, $C_3=1-C_1-C_2$ , $C_4=C_1+C_2$	0-1
$C2$	-	See description for $CI$	0-1

956  
 957



958 **Table 3.** Comparisons of the model performance produced by three calibration variants.

<b>calibration variant</b>	<b>Number of behavior parameter sets</b>	<b>period</b>	<b>NSE<sub>dis</sub><sup>a</sup></b>	<b>MAE<sub>SCA</sub></b>	<b>MAE<sub>iso</sub></b>
Single-objective	126	calibration	0.79 (0.75-0.84)	0.25 (0.08-0.78)	2.21 (0.66-4.10)
		validation	0.79 (0.71-0.84)	0.24 (0.07-0.79)	2.53 (0.77-4.88)
Dual-objective	117	calibration	0.79 (0.75-0.85)	0.10 (0.08-0.18)	2.18 (0.73-4.71)
		validation	0.80 (0.73-0.84)	0.08 (0.06-0.19)	2.38 (0.84-4.96)
Triple-objective	19	calibration	0.74 (0.70-0.81)	0.13 (0.08-0.18)	0.68 (0.48-0.83)
		validation	0.79 (0.73-0.84)	0.11 (0.06-0.18)	0.93 (0.72-1.19)

959 a: Bracketed values represent the minimal and maximal values produced by the behavioral parameter  
 960 sets.

961



962 **Table 4.** Average percentages of water sources in the annual water input for runoff generation.

	Single-objective	Dual-objective	Triple-objective
Rainfall	48.0	44.2	47.4
Snow melt	19.7	22.0	23.4
Glacier melt	32.2	33.8	29.2
Uncertainty <sup>a</sup>	12.4	9.4	6.2

963 a: The uncertainty of the contribution is defined as  $E = \sqrt{E_R^2 + E_N^2 + E_G^2}$ , where  $E_R$ ,  $E_N$  and  $E_G$   
964 represent the standard deviations of the contributions of the water sources produced by the corresponding  
965 behavioral parameter sets. Subscripts of  $R$ ,  $N$  and  $G$  represent rainfall, snow meltwater and glacier  
966 meltwater, respectively.  
967



968 **Table 5.** Simulated contributions of runoff components to annual runoff

	Single-objective	Dual-objective	Triple-objective
Surface runoff	65.9%	66.4%	64.9%
Subsurface runoff	34.1%	33.6%	35.1%
Uncertainty <sup>a</sup>	11.8%	12.1%	4.1%

969 a: The uncertainties of the contributions were calculated in the same way in Table 4.